

Article

An Accurate Recognition Method for Landslides Based on a Semi-Supervised Generative Adversarial Network: A Case Study in Lanzhou City

Wenjuan Lu, Zhan'ao Zhao, Xi Mao * and Yao Cheng

Institute of Geographic Information Systems (GIS), Chinese Academy of Surveying and Mapping, Beijing 100039, China; luwj@casm.ac.cn (W.L.)

* Correspondence: maoxi@casm.ac.cn

Abstract: With the development of computer technology, landslide recognition based on machine learning methods has been widely applied in geological disaster management and research. However, in landslide identification, the problems of an insufficient number of samples and an imbalance of samples are often ignored; that is, landslide samples are much smaller than non-landslide samples. In order to solve this problem, taking the main urban area of Lanzhou City as an example, this paper proposes to construct a semi-supervised generated countermeasure network (SSGAN) model, which aims to achieve high performance with a limited number of labeled samples for precise landslide identification, and to help prevent and reduce the harm caused by disasters. In order to express the environmental characteristics of landslide development and the optical texture features of landslide occurrence, the study constructs three sets of samples to represent landslide features, including a landslide influencing factor sample set, a Sentinel-2A optical remote sensing sample set, a joint influencing factor and Sentinel-2A sample set. The three kinds of sample sets are transferred to SSGAN for training to form a comparative study. The results show that the joint sample set has excellent feature results in discriminator and generator. Through the experimental comparison, the model proposed in this paper is compared with the model without semi-supervised generated confrontation training. The experimental results show that the proposed method is better than the unsupervised adversarial learning model in terms of accuracy, F1 score, Kappa coefficient, and MIoU. A total of 160 landslides have been identified in the study area, with a total area of 10.328 km², with an accuracy rate of 83%. Therefore, the generated results are accurate and reliable, and show that SSGAN can better distinguish landslides from non-landslides in an image, under the condition of obtaining a large number of unmarked environmental features; enhance the effect of landslide classification in complex geographical environment; and then put forward effective suggestions for the prevention and control of landslides and geological disasters in the main urban area of Lanzhou.



Citation: Lu, W.; Zhao, Z.; Mao, X.; Cheng, Y. An Accurate Recognition Method for Landslides Based on a Semi-Supervised Generative Adversarial Network: A Case Study in Lanzhou City. *Appl. Sci.* **2024**, *14*, 5084. <https://doi.org/10.3390/app14125084>

Academic Editor: Yosoon Choi

Received: 26 April 2024

Revised: 31 May 2024

Accepted: 8 June 2024

Published: 11 June 2024

Keywords: semi-supervised learning; generative adversarial networks; landslide recognition; machine learning; insufficient samples

1. Introduction

China, with its vast territory and diverse geological environment, faces a wide distribution of disasters, including the frequent occurrence of landslides [1]. Therefore, the prevention and control of landslide disasters should focus on early identification and detection warning research rather than post-disaster management.

In recent years, various techniques have been developed for landslide identification and evaluation. Common methods include probability analysis based on landslide inventories [2], reasoning based on empirical knowledge [3], mathematical models based on physical mechanics [4], and statistical methods based on data [5]. On the basis of traditional linear statistical analysis, with the development of computer technology, machine learning



Copyright: © 2024 by the authors. Licensee MDPI, Basel, Switzerland. This article is an open access article distributed under the terms and conditions of the Creative Commons Attribution (CC BY) license (<https://creativecommons.org/licenses/by/4.0/>).

methods have emerged as prominent techniques due to their autonomous analysis capabilities for large amounts of data [6]. Methods such as random forests [7], support vector machines [8], logistic regression [9], and others have been applied to landslide identification. However, in complex scenarios or with higher accuracy requirements, traditional machine learning algorithms have difficulty meeting actual needs, and problems such as model overfitting and easy trapping in local optima still exist [10]. Deep learning technology, as a further development of artificial neural networks in machine learning, has also been explored by some scholars using such methods. For instance, Ju Yuanzhen [11] employed the Mask Region Convolutional Neural Network (Mask R-CNN) for the automatic identification of loess landslides using Google Earth images. Similarly, Ghorbanzadeh et al. [12] used CNNs to landslide recognition in the southern region of Rasuwa District, Nepal, and compared their results with traditional machine learning methods, highlighting the advantages of deep learning in landslide recognition.

The training process in deep learning can be categorized into two main types: supervised learning and unsupervised learning. Currently, traditional deep learning methods for landslide identification mostly adopt supervised learning [13,14], with problems such as insufficient landslide samples, imbalanced samples, and limited accuracy results. While research on landslide identification using unsupervised learning often involves processes that are difficult to understand and explain, it is difficult to estimate learning effects and performance, making it difficult to further optimize [15,16]. As a result, both supervised and unsupervised learning approaches have inherent limitations in landslide recognition tasks. Semi-supervised learning offers a promising alternative, albeit with relatively limited research to date. Therefore, this paper adopts a semi-supervised generative adversarial network to tackle the recognition task. This approach effectively addresses the issues of insufficient landslide samples and sample imbalances, ultimately enhancing the accuracy of landslide recognition and improving generalization.

This paper selects the main urban area of Lanzhou City, covering about 1631 km², as the study area. The area is located in the transition zone from the Qinghai–Tibet Plateau to the Loess Plateau, with complex terrain and geological environment, which is a typical disaster-prone area [17]. At the same time, Lanzhou has a dense transportation network and large population flows. Frequent human activities such as engineering construction and mineral resource exploitation have also become important causes of landslide disasters [18,19].

In the study of landslide disasters, the selection of influencing factors has a significant impact on the accuracy of landslide identification results. There are hundreds of factors that can affect landslides, categorized into the geomorphological and geological, human activity, and environmental conditions. Based on previous studies and the actual situation in the study area, this paper selects 10 landslide image factors as the sample set for the landslide identification task, and proposes to construct a semi-supervised generative adversarial network (SSGAN) to identify potential landslide hazards in the main urban area of Lanzhou City, develop a landslide identification program, and provide reference for landslide hazard identification in similar geological areas such as the main urban area of Lanzhou City.

2. Study the Regional Profile and Data Sources

2.1. Study Area Description

Lanzhou is located at 35°34′20″ N–37°07′07″ N and 102°35′58″ E–104°34′29″ E, which lies at the transition area between the Qinghai–Tibet Plateau and the Loess Plateau, with undulating terrain and a complex geologic environment. Lanzhou was built according to the east–west flow of the Yellow River. It is surrounded by two mountains in the south and north. It has the characteristics of a Belt Basin city. And the climate there is temperate continental with hot, rainy summers and cold, dry winters [20]. In the urban area, Quaternary aeolian loess, with vertical joints and loose structure, is the main one. And, especially in the rainy season, the urban area is liable to collapse, which makes it a typical disaster-prone area [21]. When a landslide does occur, it will pose a great

threat to the residents and facilities of the city. Therefore, it is necessary to carry out early investigation and management of hidden danger areas for disaster-prone cities such as the key urban areas of Lanzhou. This study takes the main urban area of Lanzhou City, including Chengguan District, Anning District, Xigu District, and Qilihe District as the research object to study the identification of landslides. Figure 1 shows the location of historical landslide points detected through aerial image recognition technology and ground survey and field survey techniques. These landslide sites cover various types of landslides, including loess landslides and rainfall-induced landslides. After careful identification and analysis, we have determined a total of 152 landslides, which are clearly marked on the map.

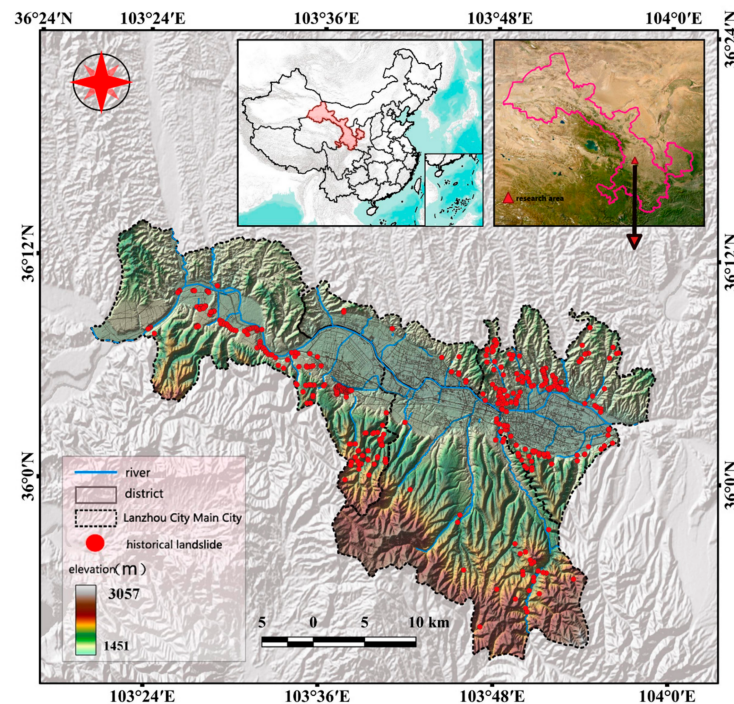


Figure 1. Overview of the study area.

2.2. Data Sources

2.2.1. Sentinel-2A Data

The Sentinel-2A remote sensing data used in this study were obtained from the United States Geological Survey (USGS). Sentinel-2A is a high-resolution multispectral imaging satellite, equipped with a multispectral instrument (MSI) [22]. It operates at an altitude of 786 km and has a swath width of 290 km, allowing it to capture data across 13 spectral bands, providing rich spectral information. The Sentinel-2A sensor covers the visible, near-infrared, and shortwave-infrared spectral regions [23]. The data have three spatial resolutions: 10 m, 20 m, and 60 m. The detailed sensor parameters are shown in Table 1.

Table 1. Sentinel-2A sensor parameters.

Sensor	Wave Band	Central Wavelength (μm)	Resolution Ratio (m)
MSI	Band 1—super blue (coastal and aerosol)	0.443	60
MSI	Band 2—blue	0.490	10
MSI	Band 3—green	0.560	10
MSI	Band 4—red	0.665	10

Table 1. *Cont.*

MSI	Band 5—visible and near-infrared light	0.705	20
MSI	Band 6—visible and near-infrared light	0.740	20
MSI	Band 7—visible and near-infrared light	0.783	20
MSI	Band 8—near-infrared light	0.842	10
MSI	Band 8A—visible and near-infrared light	0.865	20
MSI	Band 9—shortwave infrared-vapor	0.945	60
MSI	Band 10—shortwave infrared-cirrus cloud	1.375	60
MSI	Band 11—shortwave infrared	1.610	20
MSI	Band 12—shortwave infrared	2.190	20

2.2.2. Landslide Influencing Factors Data

Landslide influencing factors reflect the complex environmental characteristics that contribute to landslide development from different perspectives. There are hundreds of factors that can affect landslides, which can be divided into categories such as geomorphological, geological, human activity, and environmental conditions. Slope and elevation can provide potential energy for the occurrence of landslides [24,25]. Considering the historical cases, areas with high elevations and steep slopes in the study area are more prone to landslides. Aspect affects the degree of precipitation and solar radiation received by the region [26], which in turn influences water movement and soil properties, thereby affecting landslide occurrence. Lithology and rock types have a significant impact on the type of slope soil, slope structure, and soil shear strength [27]. Distance-based influencing factors are calculated using Euclidean distance. The distance to faults affects the mechanical structure of the landslide body, as the discontinuity of the rock and soil mass cut by various structural surfaces can create conditions for downsiding. The distance to rivers reflects the effects of surface runoff erosion and soil erosion on landslide evolution [28]. Land use and road distance reflect human utilization and modification of natural conditions, and human activities, such as road and railway construction, irrigation, and residential development, can increase the frequency and possibility of landslide disasters [29]. The Normalized Difference Vegetation Index (NDVI) is used to evaluate the growth status of surface vegetation. When the NDVI value is relatively small, it indicates poor vegetation growth and poor soil stability, which may have a higher landslide risk [30]. Rainfall is an important triggering factor for landslides, as abundant precipitation can increase the water content of the surface and subsurface, change the physical properties of the soil, reduce the soil's shear strength, and increase soil permeability, thereby exacerbating the occurrence of landslides [31].

The above landslide influencing factors all contribute to landslides in Lanzhou to varying degrees. This paper refers to common landslide influencing factors and analyzes the relationship between the geological environment, development, and distribution characteristics of landslide disasters in the study area of Lanzhou City. A total of 10 influencing factors were selected, including distance to roads, elevation, distance to faults, distance to rivers, average annual rainfall, slope, NDVI, aspect, lithology, and land use.

The construction of landslide influencing factors is shown in Figure 2. The detailed data sources and resolutions of the landslide influencing factors are shown in Table 2. Considering the size of local landslides and the available data, the spatial resolutions of 10 m, 30 m, and 50 m were selected. If the selected resolution is too high, it will

introduce noise and increase data redundancy. Conversely, a low resolution will simplify the data, leading to a decrease in landslide recognition accuracy. This study uses collinearity analysis and the random forest algorithm to determine the final landslide influencing factors for training [32].

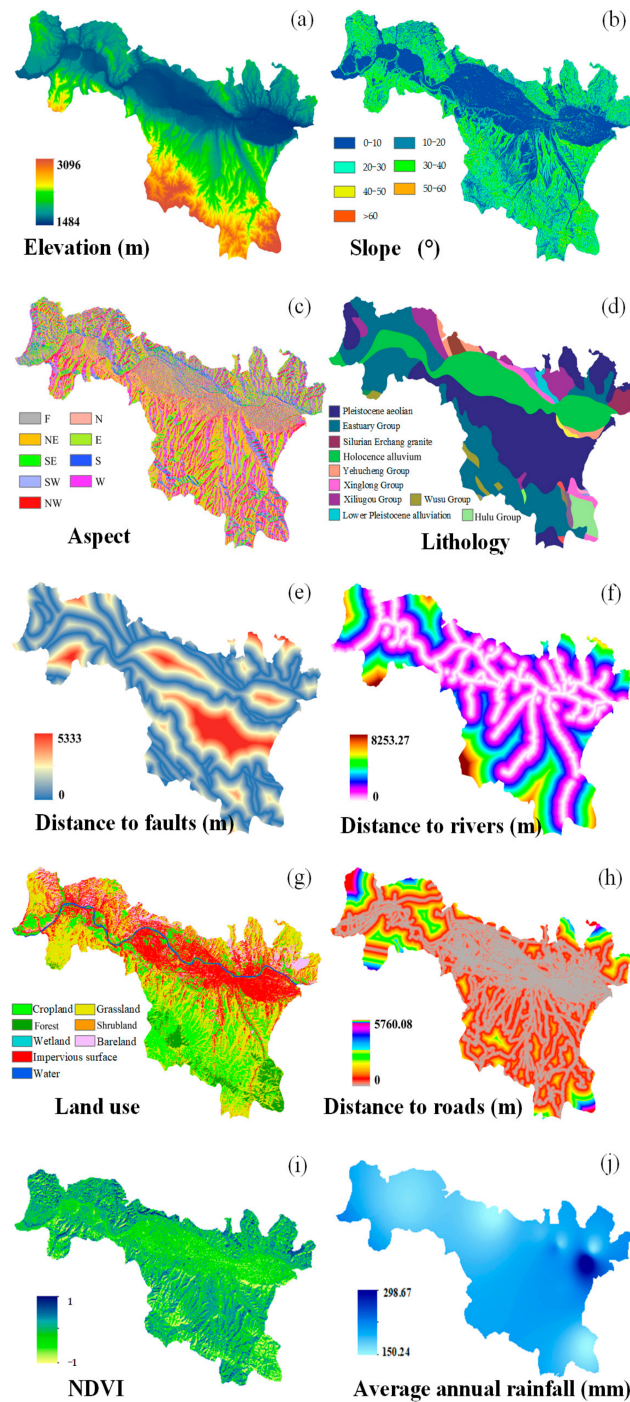


Figure 2. Influencing factors for landslides. (a) Influencing factors of elevation. (b) Influencing factors of slope. (c) Influencing factors of aspect. (d) Influencing factors of lithology. (e) Influencing factors of distance to faults. (f) Influencing factors of distance to rivers. (g) Influencing factors of land use. (h) Influencing factors of distance to roads. (i) Influencing factors of NDVI. (j) Influencing factors of average annual rainfall.

Table 2. Data Sources of Landslide Influencing Factors.

Data Name	Data Source	URL	Influencing Factor	Resolution
SRTM DEM	United States Geological Survey	http://earthexplorer.usgs.gov (26 June 2023)	Elevation Slope Aspect	30 m
Land Use	Tsinghua University	http://data.ess.tsinghua.edu.cn/ (11 September 2023)	Land use	30 m
Rainfall	Geospatial Remote Sensing Ecology Network	http://www.gisrs.cn/ (6 March 2024)	Average annual rainfall	50 m
Normalized Difference Vegetation Index	National Ecological Data Center Resource Sharing Platform	http://www.nesdc.org.cn (18 January 2024)	NDVI	10 m
Lithology and Faults	United States Geological Survey	https://www.cgs.gov.cn/ (20 December 2023)	Lithology Distance to faults	1:4,000,000 30 m
Rivers and Roads	Lanzhou Natural Resources Bureau	http://zrzyj.lanzhou.gov.cn/ (24 October 2023)	Distance to rivers Distance to roads	30 m 30 m

3. Methods for Landslide Identification

3.1. Semi-Supervised Learning

Semi-supervised learning lies between supervised and unsupervised learning, with the goal of achieving excellent performance using only a small number of labeled samples. The basic idea of semi-supervised learning is to use the distribution information of a large amount of easily accessible unlabeled data for model learning, and use a small amount of labeled data for auxiliary training, so as to achieve a model with strong generalization ability and prediction performance [33]. Common semi-supervised learning methods include self-training algorithms, co-training algorithms, and generative models. A self-training algorithm is a simple semi-supervised learning method. It trains the initial model with labeled samples, then predicts unlabeled samples with the model, adds the samples with high prediction confidence to the labeled samples, and iterates training repeatedly until the model converges [34,35]. This algorithm is easy to understand but is sensitive to label noise and errors, and is easily affected by noise and outliers in unlabeled data. A co-training algorithm uses multiple models to cross-train each other. It divides the feature space into two non-overlapping subspaces and uses one model to correct the predictions of the other model. However, it relies on the selection of classifiers and requires consistency in the distribution of labeled data; otherwise, the learning results may be unstable [36]. Generative models are a class of models that can learn data distributions and generate new data through distribution features. Due to their data generation capability, they are widely used in tasks such as sample interpolation, image generation, and text generation [37]. Generative adversarial networks (GANs) have become the most typical generative models in recent years and have become a focus of many studies [38]. Compared with traditional generative models, such as probabilistic graph models and variational autoencoders, GANs do not require an explicit definition of the likelihood function or assumptions about the distribution. They complete learning solely from the data perspective, demonstrating more sufficient applicability for semi-supervised learning [39]. Therefore, this study uses a GAN to implement semi-supervised learning for landslide identification tasks.

3.2. Generative Adversarial Network

The GAN was first proposed by scholar Goodfellow et al. in 2014 [40], drawing inspiration from game theory's two-player zero-sum game, where one player's gain is equal to the other player's loss, resulting in an overall zero-sum outcome. Since its inception, the GAN has been widely applied in fields such as image synthesis, image restoration, super-resolution, speech conversion, and has gradually become a hot topic in the field of artificial intelligence [41].

A GAN model generally contains two sub-neural networks, namely the generator (G) and discriminator (D). The two networks have opposing training targets, thus producing an

adversarial learning process. The generator can generate new samples from random noise vectors, while the discriminator is used to determine whether a sample comes from real samples or fake samples generated by the generator. The two networks continuously optimize their parameters through a feedback mechanism—the generator makes the samples it generates gradually approach the distribution of real data, while the discriminator aims to accurately distinguish real data from generated data as much as possible [42]. The model training ends when the generator can “deceive” the discriminator and the discriminator’s classification of all data tends to be stable. More specifically, the overall training idea of a GAN can be expressed in its objective function. Typically, a random noise variable z , following the standard normal distribution $z \sim N(0,1)$, is used as the input for G to obtain pseudo-samples $G(z)$. The inputs for D are the generated samples and the real samples, and its scalar output is the estimated probability that the input comes from real samples. The optimization goal of D is to make the output probability as close to 1 as possible for the inputs of real samples, and as close to 0 as possible for the inputs of generated samples. The optimization goal of G is to make the true/false judgment probability $D(G(z))$ of the generated sample $G(z)$ by D consistent with the true/false judgment probability $D(x)$ of the real sample x by D . Therefore, the optimization process is an adversarial process of minimizing G and maximizing D , constructed in the form of:

$$\min_G \max_D V(D, G) = E_{x \sim P_{data}(x)} [\log D(x)] + E_{z \sim P_{noise}(z)} [\log(1 - D(G(z)))] \quad (1)$$

where $E(*)$ represents the expected value of the distribution function, $P_{data}(x)$ represents the distribution of real samples, and $P_{noise}(x)$ is defined by the low-dimensional noise distribution.

3.3. Semi-Supervised Generative Adversarial Network Model Construction

Drawing from the concepts of semi-supervised learning and GAN theory discussed earlier, this paper introduces the development of a semi-supervised generative adversarial network (SSGAN) for the task of landslide recognition in the primary urban area of Lanzhou City. SSGAN is a semi-supervised extension of the traditional GAN framework, designed to enhance the model’s classification accuracy when there is an insufficient number of labeled samples. SSGANs have demonstrated remarkable performance on various datasets in multiple studies since their inception. For instance, Zhou et al. [43] employed a SSGAN to classify imbalanced samples, achieving an impressive accuracy rate of up to 97.52%. Miao et al. [44] effectively utilized a SSGAN to compensate for missing values in multivariate time series data. On the CIFAR-10 dataset, a SSGAN improved classification accuracy by 1–2% when compared to other semi-supervised learning methods and traditional GAN approaches. Thus, SSGANs have proven their adaptability across various semi-supervised classification tasks and exhibits substantial potential for further development. Notably, there has been no prior research applying a SSGAN to landslide recognition tasks that also face sample limitations.

The core concept of a SSGAN involves an expansion of the discriminator within a conventional GAN network, transforming an N -class classification problem into an $N + 1$ classification problem, with the additional class corresponding to generated pseudo-images. SSGAN seamlessly integrates both labeled and unlabeled samples as input. For labeled samples, the discriminator meticulously assesses the probability of belonging to one of the N predefined categories. In the case of unlabeled samples, the discriminator evaluates the likelihood of being an actual image from the overall N class. Regarding samples generated by the generator, the discriminator determines the probability of being a false image belonging to the $N + 1$ class. This configuration introduces a secondary competition between unlabeled samples and generated samples, enhancing the model’s comprehension of the real sample distribution and resulting in more precise classification outcomes. Building upon these principles, this paper has constructed an SSGAN model tailored to the task of landslide recognition within the study area. The specific model structure is illustrated in Figure 3.

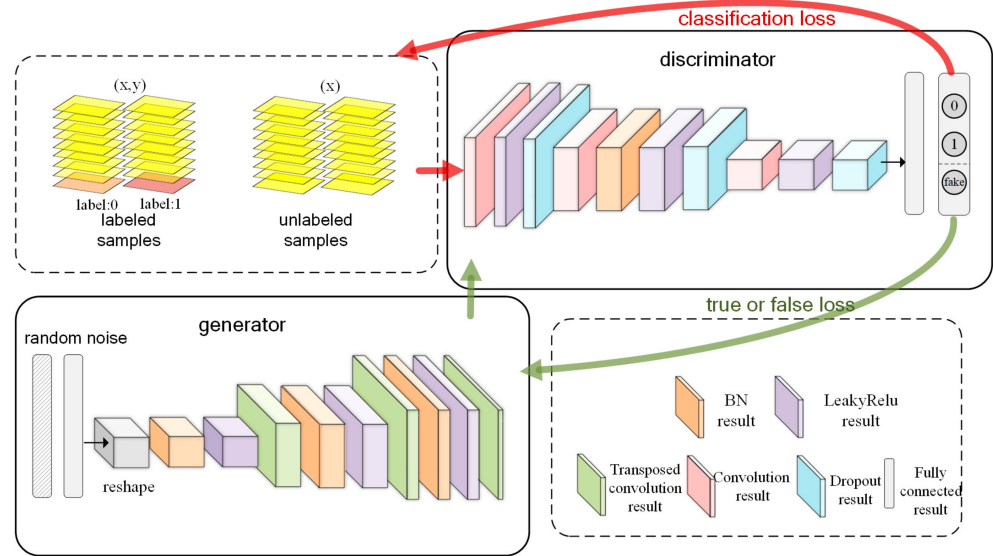


Figure 3. Semi-Supervised Generative Adversarial Network Structure. The red arrow represents the input and discriminant result of the real sample, and the green arrow represents the input and discriminant result of the generated sample. The yellow represents the factor, the red and orange are the labels. Grey represents random noise data vector and input data vector respectively.

Within the model’s discriminator component, the input data consists of generator-generated samples, samples that have been labeled as landslides and non-landslides, as well as unlabeled samples. The structure of the discriminator network adheres to the foundational feed-forward deep convolutional neural network (CNN) architecture, which is adept at extracting image features and reducing spatial dimensions. A CNN possesses robust feature learning capabilities and is widely employed in various domains, including pattern recognition and image classification [45]. A CNN comprises several key functional layers, including the convolutional layer, pooling layer, and fully connected layer. Of these, the convolutional layer is the cornerstone of a CNN network. It aggregates information through convolutional kernel operations across both spatial and feature dimensions, allowing it to capture feature details in a localized perceptual manner. In the output of the convolution operation, each point corresponds to a specific portion of the original image, referred to as the receptive field. During the forward propagation process of a CNN, as each convolutional layer reduces the size of its feature map, the amount of information contained in the feature representation gradually increases, accompanied by an expansion of the receptive field. The values of the convolutional kernel are updated during backpropagation, and multiple convolutional kernels are employed in each convolutional layer to capture diverse texture and edge features. Take the images of $n \times n \times n_c$ as the input, with n as the side length of the image and n_c the number of channels. Fill the image boundary with 0 elements with the number of p_0 , and slide in the input image using the convolution kernel with a size of $f_k \times f_k \times n_c$, and the number of n'_c at a step distance of h_c . During the sliding process, the convolution kernel and the corresponding image pixel are multiplied and then added, and the calculation result is the updated corresponding pixel value. The operation results of the input image and a convolutional layer are shown in the following formula, where the upper $[l]$ represents the first neural layer; $\lfloor \cdot \rfloor$ represents rounding down.

$$n^{[l+1]} = \left\lfloor \frac{n^{[l]} + 2p_0 - f_k}{h_c} + 1 \right\rfloor \times \left\lfloor \frac{n^{[l]} + 2p_0 - f_k}{h_c} + 1 \right\rfloor \times n'_c \quad (2)$$

The pooling layer serves a fundamental purpose in CNN by reducing the size of the feature map while preserving essential characteristic information, thus diminishing data redundancy. Following convolution and pooling operations, the CNN extracts these characteristics to construct a feature map. The incorporation of LeakyReLU activation func-

tions enhances the model's nonlinearity, preventing gradient vanishing, and consequently, improving the model's generalization capabilities. The batch normalization (BN) layer plays a crucial role in accelerating network training while enhancing the model's accuracy and robustness. The fully connected layer is typically located at the final segment of the CNN's hidden layers. It effectively discards the spatial topological relationships within the feature map, converting it into a series of vector-based features. These features are then propagated to the output layer through an activation function. In this particular study, the discriminator ultimately generates three output neurons via the fully connected layer, corresponding to the three categories: non-landslide (0), landslide (1), and fake.

The input to the generator is composed of random noise adhering to a normal distribution. This noise undergoes reshaping before being upsampled through transposed convolution. The feature map produced via transposed convolution is progressively remapped to the spatial domain of the original input image. This meticulous process guarantees that the generated image attains a semantic level of interpretation by the discriminator, matching the pixel-level fidelity of an authentic image. The calculation for determining the output feature map size resulting from the transposed convolution operation can be expressed using Formula (3). In this formula, 'k' represents the size of the convolution kernel, 's' indicates the stride, and 'p' denotes image boundary padding. During this operation, both LeakyReLU activation and the batch normalization (BN) layer are applied to expedite the training process and enhance the model's stability

$$n^{[l+1]} = \lfloor s(i-1) + 2p - k + 2 \rfloor \times \lfloor s(i-1) + 2p - k - 2 \rfloor \times n'_c \quad (3)$$

From the perspective of loss function, the model built in this paper mainly uses two types of losses: binary cross-entropy (BCE) and multi-class cross-entropy (MCE). BCE is used to measure the gap between the predicted value of the model and the real label in the binary classification problem, and the calculation is shown in Formula (4), where y is the real label of the sample (the value is 0 or 1), and \hat{y} is the output category probability value of the model. MCE is an extension of BCE, and its calculation is shown in Formula (5), where N represents the number of classification categories. In the loss function of the model, MCE is taken to judge the category loss for real samples, and BCE is used to judge the true and false losses for generated samples and unlabeled samples. The discriminator loss generally includes three types of losses: labeled sample class loss, unlabeled sample true and false losses, and generated sample true and false losses. Generator losses include a category of true and false losses.

$$L_{BCE}(y, \hat{y}) = -(y \log \hat{y} + (1 - y) \log(1 - \hat{y})) \quad (4)$$

$$L_{MCE}(y, \hat{y}) = -\sum_{i=1}^N y_i \log \hat{y}_i \quad (5)$$

3.4. Verification Method

3.4.1. Landslide Factor Analysis

When studying the regression relationship between landslides and their influencing factors, it is first necessary to ensure the independence of the factors. When there is a strong linear relationship between the factors, it becomes difficult to find the true relationship between a single factor and the occurrence of landslides, leading to large biases or even opposite results in the model's prediction, a phenomenon known as multicollinearity among the factors.

Multicollinearity is usually tested using the variance inflation factor (VIF) and tolerance (T) methods to check the collinearity of the influencing factors [46–48], with the calculation formulas as follows:

$$VIF = \frac{1}{1 - A^2} = \frac{1}{T} \quad (6)$$

In the equation, A^2 represents the complex correlation coefficient of a specific independent variable when a regression analysis is conducted with the other independent variables.

When this variable exhibits a high degree of correlation with the remaining variables, the value of A^2 approaches 1, resulting in a larger value for VIF (variance inflation factor). If the VIF exceeds 10 and its reciprocal, tolerance (T), is less than 0.1, it indicates the presence of multicollinearity.

3.4.2. Precision Analysis

The model must first have the premise of accurate recognition of the sample landslide to ensure the reliability of the final recognition results. In order to quantitatively evaluate the results of landslide recognition, this paper uses the commonly used indicators in the semantic segmentation problem to interpret the results. The confusion matrix is a basic and widely used approach [49] and it was built as shown in Table 3. When calculating the confusion matrix, the research uses the test set data for verification. The test set data are unknown to the trained model, which helps to objectively evaluate the model's learning of landslide characteristics. In the test set, landslide samples are treated as positive samples, and non-landslide samples are treated as negative samples.

Table 3. Confusion Matrix.

Confusion Matrix		Predicted Value	
		Positive Example (+)	Counter Example (−)
True value	Positive example (+)	True Positive TP	False Negative FN
	Counter example (−)	False Positive FP	True Negative TN

TP, FN, FP, and TN represent the quantity of predicted results of the model divided by threshold values in four different scenarios. Using these values, the following indicators can be calculated:

Precision is used to measure the ratio of the correct target to the judged correct target, that is, the proportion of correct (true label positive) samples in all samples judged positive by the model. The calculation formula is as follows:

$$Precision = \frac{TP}{TP + FP} \quad (7)$$

Recall is a metric that quantifies the percentage of correctly identified positive instances out of all actual positive instances. It essentially measures the ability of a model to capture all relevant instances in the dataset.

$$Recall = \frac{TP}{TP + FN} \quad (8)$$

The F1-score represents the weighted harmonic mean of precision and recall, effectively balancing the influence of both metrics. This measure provides a more holistic view of a model's performance by simultaneously considering both the precision (the accuracy of positive predictions) and the recall (the model's ability to identify all relevant instances). A higher F1-score indicates superior performance of the model, showcasing its effectiveness in accurately and comprehensively identifying positive instances.

$$F1 - \text{score} = \frac{2 \times R \times P}{R + P} = \frac{2 \times TP}{2 \times TP + FP + FN} \quad (9)$$

The Kappa coefficient serves as a measure to validate the agreement between model predictions and actual outcomes. In the context of classification problems, this agreement

pertains to the consistency between the results derived from model assessments and the true classification outcomes.

$$Kappa = \frac{N \sum_{i=1}^n X_{ii} - \sum_{i=1}^n (X_{i+} X_{+i})}{N^2 - \sum_{i=1}^n (X_{i+} X_{+i})} \quad (10)$$

where n is the sum of the number of rows in the confusion matrix (the total number of categories); X_{ii} is the number of samples in i row and i column in the confusion matrix, that is, the number of samples correctly classified; X_{i+} and X_{+i} are the total number of samples in row i and column i , respectively; N is the total number of samples used for accuracy evaluation. Mean intersection over union (MIoU) is the standard evaluation index of semantic segmentation networks and is the mean of the sum of the ratios of intersection and union between the predicted results of each category of the model and the real labels.

$$MIoU = \frac{\frac{TP}{FP+TP+FN} + \frac{TN}{FP+TN+FN}}{2} \quad (11)$$

4. Accurate Recognition of Landslides Based on Semi-Supervised Generative Adversarial Network

4.1. Dataset Building

In order to express the environmental characteristics of landslide development and the optical texture features of landslide occurrence, this paper proposes to construct three kinds of sample sets representing landslide characteristics, which are the landslide influence factor sample set, the Sentinel-2A optical remote sensing sample set, and the joint influencing factor and Sentinel-2A sample set. These three kinds of sample set form a comparative study for landslide identification and analysis.

For each type of feature sample set, the sample is obtained in the same way. In order to achieve the purpose of pixel-level discrimination, this paper proposes a sliding cutting strategy to construct a single sample, and the production process is shown in Figure 4. The specific methods are as follows: first of all, 10 environmental image factor features, 12 band optical feature datasets, and historical landslide distribution maps are converted to the same resolution. Sentinel-2A imagery is used as the reference for resampling all image factors to a 10 m resolution. The selected feature data and the historical landslide distribution map are combined to create the original dataset, comprising pixel images with dimensions of 4314 rows and 7210 columns. A 13×13 pixel window is used to slide across the image, covering every pixel in the image. This synchronized sliding window cutting for image factors, optical images, and historical landslide images ensures that all features correspond to the original landslide area, creating individual image samples. The labeled data sample set assigns labels based on the pixel value at the original landslide center point, with landslide points labeled as 1 and non-landslide points labeled as 0. The unlabeled sample set is obtained from non-landslide locations to enable the model to learn the characteristics of the actual environment. Among all the image samples generated through cutting, 89,160 landslide samples, an equal number of non-landslide samples, and an equal number of unlabeled data samples, are randomly selected. Finally, the landslide samples, non-landslide samples, and unlabeled samples form the dataset, which is then divided into a model training set and a test set in a 7:3 ratio. This ratio is widely adopted in practice and has been proven to be effective. The training set is used for the model to learn the characteristics of landslides and train the internal parameters of the model, while the test set is used to assess the final generalization error of the model and evaluate its robustness.

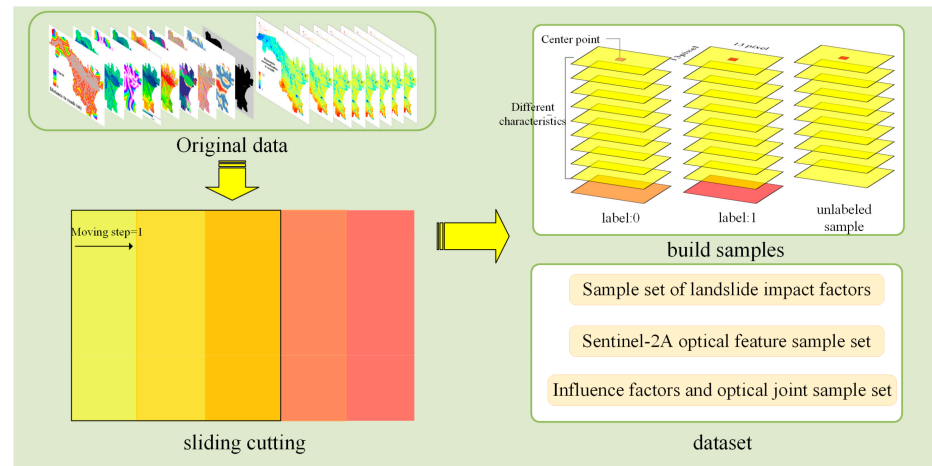


Figure 4. Production strategy of sliding cutting sample.

4.2. Understanding and Analysis of Semi-Supervised Generative Adversarial Processes

To compare and analyze the learning performance of different features in the model and select appropriate learning samples, this paper separately feeds the landslide influencing factors sample set, Sentinel-2A optical remote sensing sample set, and the joint sample set combining influencing factors and Sentinel-2A data into the semi-supervised generative adversarial network (SSGAN). It evaluates the model's ability to complete landslide recognition tasks through training with different data inputs. In this comparative study, all model hyperparameters and the number of iterations are kept constant, ensuring a fair evaluation. The experiments were conducted in Python using the TensorFlow framework on a host system equipped with an Intel Xeon Silver 4214 processor and NVIDIA Quadro P2200 graphics card (NVIDIA, Santa Clara, CA, USA).

Regarding the discriminator, Figure 5 illustrates the loss function curve during the discriminator's training process. The study decomposes the total loss of the SSGAN discriminator, which is designed for $N + 1$ class classification, into three parts: real sample classification loss, unlabeled sample true and false loss, and generated sample true and false loss. This breakdown allows for a more in-depth understanding of the discriminator's performance in different functions.

When training with the influencing factor sample set, the true and false loss for generated and unlabeled samples stabilizes after a small number of iterations, indicating that the model quickly recognizes true and false samples. However, the overall loss function remains relatively high. This might be attributed to a high learning rate for the generator and the relatively simple distribution of influencing factor data, resulting in rapid convergence for true and false judgments and a continuous decrease in the model's classification loss for true labeled samples. After 100 iterations, the loss for true labeled samples reaches approximately 0.276, indicating improved classification performance.

In contrast, when using optical image datasets, the loss in determining the authenticity of generated and unlabeled samples fluctuates significantly. Initially, there is a sharp decrease, followed by a continuous upward trend. This behavior may be due to the high resolution of optical images, which introduces more image noise and a complex feature distribution. This complexity can lead to generator instability, making it challenging for the discriminator to accurately distinguish between samples generated by the generator and labeled samples. Consequently, the model struggles to correctly interpret environmental features, resulting in suboptimal classification performance for labeled samples.

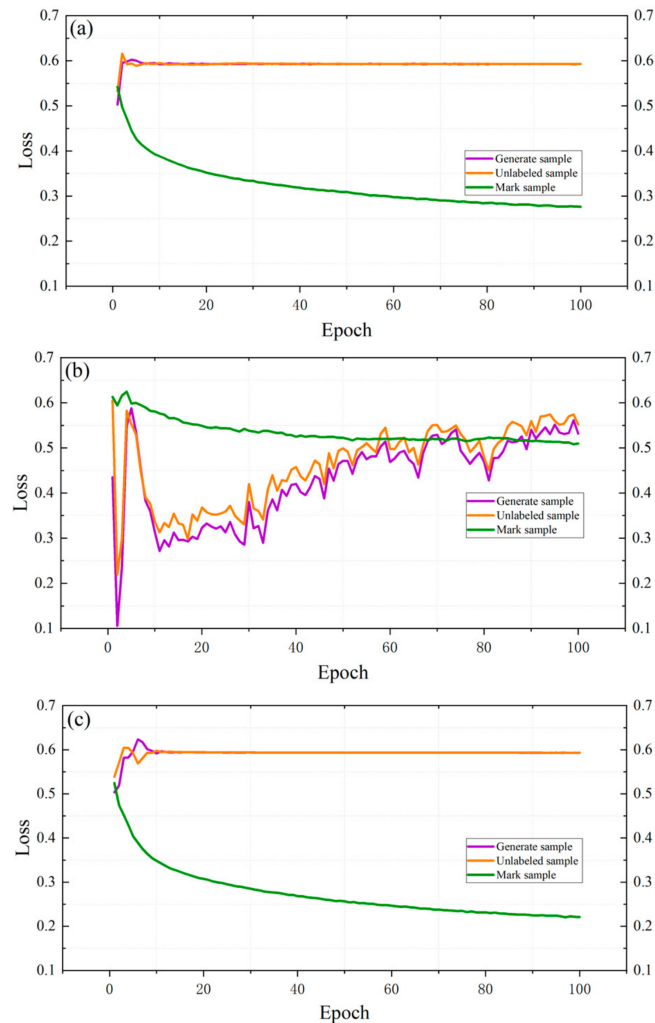


Figure 5. Comparison of Discriminator Training Process. (a) Sample set of landslide impact factors. (b) Sentinel-2A optical remote sensing sample set. (c) Joint sample set.

For the joint sample set, the model effectively mitigates the issues encountered in optical image training. The judgment of true and false images remains relatively stable, and the loss, although still high, stays below 0.6 overall, which falls within an acceptable range for deep learning model training. Notably, the classification loss for labeled samples is significantly reduced compared to using only influencing factor features, reaching around 0.221 after 100 iterations. These results indicate that the model's performance is promising and will be valuable for landslide classification tasks.

In terms of generators, this paper sets fixed random noise seeds during the training process to output the generator generated image results after a specific round of iterations. Some of the results are shown in Figure 6. On three types of datasets, the generator gradually generates results similar to the real data distribution as the number of iterations increases; however, with slight differences. From a more intuitive point of view, using optical image datasets to generate results with more noise is consistent with the discriminator training curve. The overall results of using the joint dataset are clearer and closer to the real sample.

Based on the performance comparison of SSGAN on three types of datasets in both the discriminator and the generator, it can be inferred that completing semi-supervised landslide recognition tasks solely relying on optical images poses challenges. However, the model demonstrates better performance when combining optical images with image factor features compared to using only influencing factor features. Therefore, in light of these

findings, this paper will utilize the training results from the joint sample set for subsequent landslide recognition tasks, aiming to deliver more accurate and reliable outcomes.

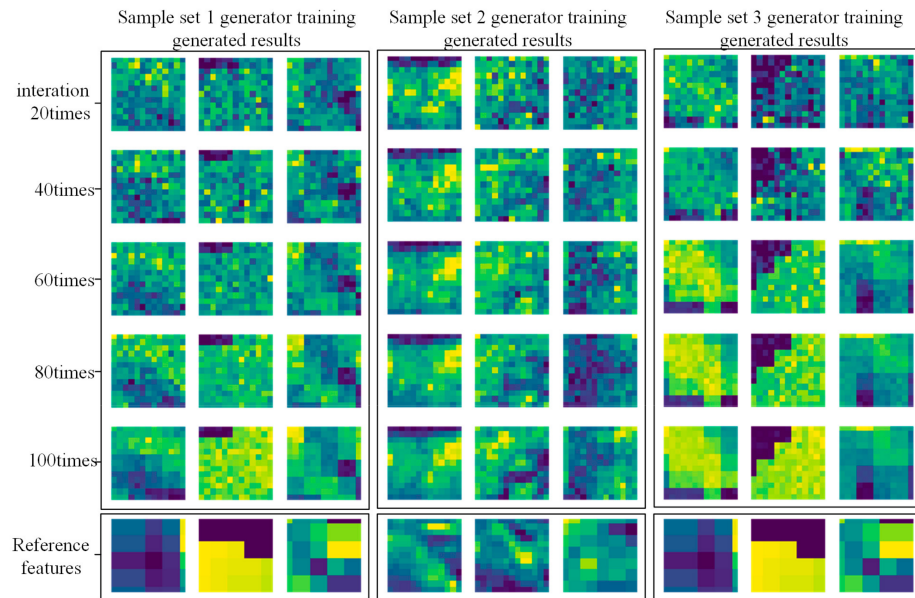


Figure 6. Comparison of generator training results.

5. Results and Discussion

5.1. Characteristic Analysis of Landslide Factors

The results of multicollinearity analysis are depicted in Figure 7. The VIF values for the ten selected landslide influencing factors in this study fall within the range of 1–3. The maximum VIF value (2.189) is observed for the distance to rivers, while the minimum value (1.036) is associated with average annual rainfall. The tolerance values range from 0.4 to 1, with a maximum value of 0.965 and a minimum of 0.457. These results indicate that all ten selected influencing factors satisfy the critical value criteria for VIF and Tolerance. This suggests that they exhibit good independence and do not suffer from collinearity issues. In summary, the ten influencing factors chosen in this study can be confidently utilized in subsequent model training and result evaluation, ensuring the data’s validity and accuracy.

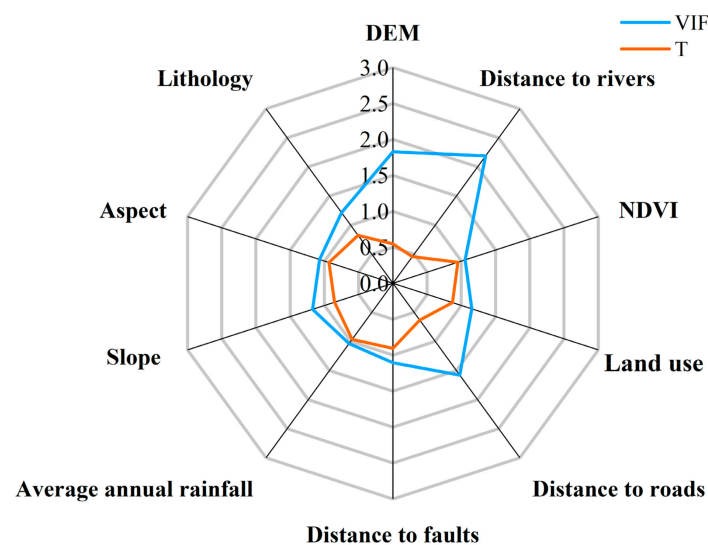


Figure 7. Multicollinearity analysis results of landslide influencing factors.

Upon verifying the suitability of the chosen factors, the study seeks to acquire an initial insight into the manner in which these factors impact landslides. To this end, the random forest (RF) algorithm is utilized to prioritize the selected influencing factors according to their significance in feature importance. RF is a widely used method in the realms of data mining and feature selection. It reduces model variance by aggregating predictions from multiple decision trees, demonstrating robustness against outliers and noise, handling high-dimensional data effectively, analyzing nonlinear, collinear, and interactive data, and providing variable importance scores during data analysis [50,51]. In this paper, the importance score of different factors in relation to landslide occurrence is calculated using the out-of-bag (OOB) error rate method within the RF framework. The results are then sorted in descending order of importance. The ranked factors are as follows: distance to roads (0.1716), elevation (0.1664), distance to faults (0.1593), distance to rivers (0.1285), average annual rainfall (0.1129), slope (0.0888), NDVI (Normalized Difference Vegetation Index) (0.0584), aspect (0.0500), lithology (0.0455), and land use (0.0189). Notably, distance to the roads emerges as the most critical factor, underscoring the significant impact of human engineering activities on landslide occurrence. Elevation and the presence of faults create conditions conducive to landslides. Meanwhile, rivers and rainfall contribute to landslides by influencing soil structure, while the other factors exhibit varying degrees of association with landslide occurrence. It is worth noting that the landslide samples mentioned in this research are not solely based on their proximity to human activity areas, but rather obtained through the use of remote sensing interpretation technology from a broader geographic range. Meanwhile, the purpose of the landslide susceptibility assessment is to better prevent landslides that may pose a threat to humans. Landslide samples in remote areas may be relatively fewer, so they have a limited impact on the main purpose of this research. It is precisely based on this comprehensive data collection approach and clear research focus that the results of the ranking of the importance of landslide influencing factors are reasonable.

5.2. Landslide Recognition Results

This paper utilized the trained model to conduct supplementary landslide recognition in the main urban area of Lanzhou City. To demonstrate the effectiveness of semi-supervised generative adversarial learning, a comparative study was conducted using a model that only includes the discriminator part of SSGAN. This comparative model takes labeled samples as input and outputs two classification results, while keeping other hyperparameters consistent with SSGAN. After pixel-level recognition, to align with the actual development of landslides, the generated results were clustered and smoothed. The landslide recognition results of the two models are depicted in Figure 8a illustrates that the model without semi-supervised generative adversarial training (GAN) recognized 204 landslides, including constraint recognition results, covering a total area of 10.913 km². SSGAN identified 160 landslides in the study area, the minimum landslide area identified is 68 m² and the maximum is 0.68 km², the total area is 10.328 km², which is 3.139 km² more than the recognition results of the landslide constraints, as shown in Figure 8b. From Figure 8, it is evident that more small landslides were identified without the adversarial learning model. The SSGAN recognition results align closely with the distribution of the sample landslides, providing more detailed information about the landslide edges, and even capturing some individual landslides that exceed the original landslide areas. Both methods identified more landslides than the original sample.

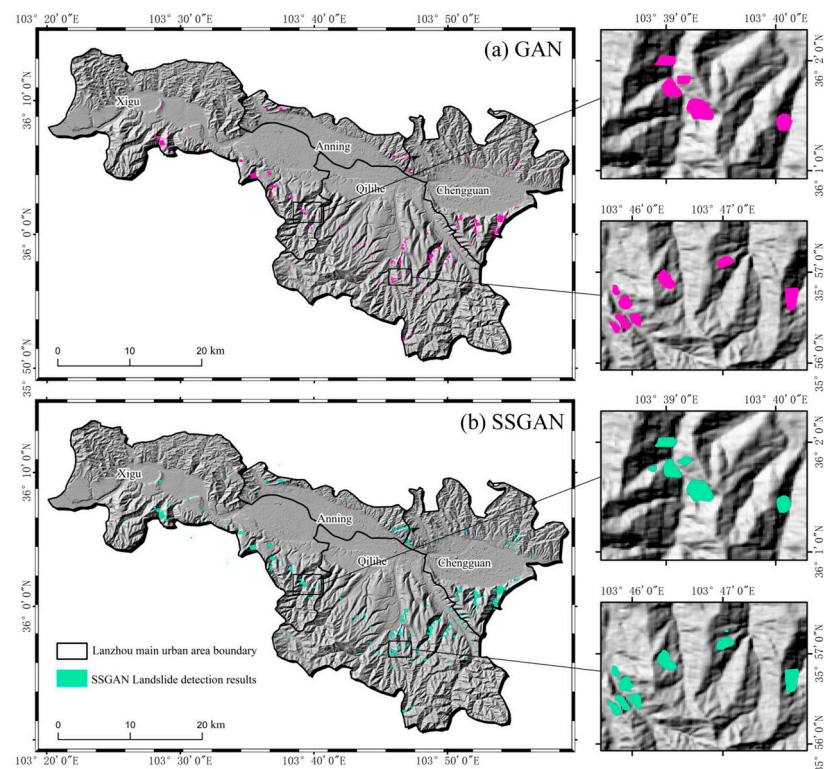


Figure 8. Comparison of accurate landslide recognition results in the main urban area of Lanzhou City: (a) GAN; (b) SSGAN. Pink represents the accurate landslide recognition results by GAN, green represents the accurate landslide recognition results by SSGAN.

Based on the above accuracy analysis and evaluation indicators, Table 4 presents the quantitative results for two distinct models, Model a represents the result of the traditional network generated by adversarial learning without semi-supervision (GAN), and Model b represents the results obtained by SSGAN used herein:

Table 4. Comparison of landslide recognition and evaluation indicators.

	Precision	Recall	F1 Score	Kappa Coefficient	MIoU
Model a (GAN)	0.795	0.961	0.860	0.858	0.887
Model b (SSGAN)	0.829	0.952	0.879	0.878	0.899

Lanzhou City primarily experiences mixed, mid-level, and small loess landslides, with the landslide body composed mainly of loess and secondary loess of various origins. These landslides exhibit spectral and textural characteristics highly similar to the surrounding environment, posing significant challenges to their accurate identification. The method proposed in this paper outperforms the model without semi-supervised adversarial learning across four comprehensive evaluation metrics: precision, F1 score, Kappa coefficient, and MIoU. However, the latter model achieves a higher recall rate of 96.09%. Recall rate measures the detection coverage of the detector on all targets to be detected, and the higher recall rate suggests that the model may be sensitive to data noise, erroneously classifying other ground features as small landslides. This results in a higher recall rate but lower accuracy rate. It is worth noting that the evaluation of a deep learning model should consider several indicators, the synthesis of these indicators furnishes a more holistic appraisal of the model's performance. Based on the five indicators quantified in this study, the model proposed in this paper exhibits a better balance and overall performance. When

provided with a substantial amount of unlabeled environmental features, semi-supervised generative adversarial learning helps distinguish landslides from non-landslides in images and reduces the false detection rate of landslides in complex geographical environments. Consequently, the model presented in this paper emerges as a dependable tool for landslide extraction, streamlining the creation of an accurate landslide database crucial for landslide identification. Although the performance improvement of the method in this research is only slight compared to Model a, its significance should not be overlooked. Particularly in addressing the challenging problem of landslide sample imbalance, the method in this research has demonstrated its effectiveness and applicability. This small improvement may seem negligible, but in real-world applications, every bit of performance enhancement can lead to more accurately predicted landslide events, thereby helping to reduce potential disaster risks. More noteworthy is that the method proposed in this research not only provides substantial contributions to current research, but also opens up new ideas and directions for future researchers.

6. Conclusions

This paper aims to utilize deep learning methods to actively learn landslide features and conduct automatic landslide identification in the research area. To overcome the challenges of insufficient landslide samples and imbalanced samples in traditional deep learning-based landslide identification, this paper proposes to construct a semi-supervised generative adversarial network (SSGAN) based on the foundation of convolutional neural networks (CNNs), in order to complete the landslide identification task.

This paper explores the feature sample sets applicable to landslide identification tasks, including the landslide influencing factor sample set, Sentinel-2A optical remote sensing sample set, and the combined sample set of influencing factors and optical features. These three sample sets are separately input into the SSGAN for training. The results show that the combined sample set has superior performance in both the discriminator and generator, so the network trained with this data set is used for further landslide identification tasks. To demonstrate the outstanding performance of SSGAN in landslide identification tasks, the identification stage uses a model that has not undergone semi-supervised adversarial training as a comparison. The proposed method in this study exhibits superior performance in the evaluation of metrics, indicating the accuracy and reliability of the generated results. After deep learning-based landslide identification, a total of 160 landslides with a total area of 10.328 km² were identified in the research area, which to some extent improves the landslide identification accuracy. In summary, the semi-supervised generative adversarial network method is a highly reliable landslide identification approach, which can provide a reference for landslide hazard identification in the main urban area of Lanzhou and similar working conditions.

This paper attempts to use SSGAN to identify landslides, and some results have been achieved. However, due to time constraints, we have not yet implemented more advanced GAN optimization methods, such as gradient penalty and feature matching and the landslide recognition results did not clearly distinguish landslides by type. In follow-up research, we will discuss these optimization techniques in depth in order to improve the ability to understand the characteristics of landslides, so as to obtain more accurate landslide recognition results.

Author Contributions: Conceptualization, methodology and validation are W.L., X.M. and Z.Z. Investigation and data curation are Y.C. Original draft preparation is W.L., review and editing are all authors. Supervision is W.L. and Z.Z., project administration is X.M. All authors have read and agreed to the published version of the manuscript.

Funding: This work was supported by the National Key Research and Development Program of China (Grant No. 2023YFF0611901) and the Exploration of Global Intelligent Positioning of Multilingual Place Names (Grant No. AR2412).

Institutional Review Board Statement: Not applicable.

Informed Consent Statement: Not applicable.

Data Availability Statement: The data presented in this study are available on request from the corresponding author. The data are not publicly available due to privacy.

Conflicts of Interest: The authors declare no conflict of interest.

References

1. Yue, S. Research on Landslide Identification Technology Based on Multi-Source Remote Sensing Data. Master's Thesis, Chang'an University, Chang'an, China, 2023.
2. Wang, Y.; Fang, Z.; Niu, R.; Peng, L. Analysis of landslide susceptibility based on deep learning. *J. Geo-Inf. Sci.* **2021**, *23*, 2244–2260.
3. Niu, P. Evaluation of Landslide Susceptibility in Zhouqu County Based on a Comprehensive Index Model. Master's Thesis, Hebei University of Geosciences, Shijiazhuang, China, 2021.
4. Chen, S.; Miao, Z.; Wu, L. Simplified Newmark displacement method for rapid assessment of seismic landslide hazard based on modified rock and soil strength parameters. *J. Seismol.* **2022**, *44*, 512–527.
5. Huang, F.; Huang, J.; Jiang, S.; Zhou, C. Landslide displacement prediction based on multivariate chaotic model and extreme learning machine. *Eng. Geol.* **2017**, *218*, 173–186. [[CrossRef](#)]
6. Ma, Z.; Mei, G.; Piccialli, F. Machine learning for landslides prevention: A survey. *Neural Comput. Appl.* **2021**, *33*, 10881–10907. [[CrossRef](#)]
7. Dou, J.; Yunus, A.P.; Tien Bui, D.; Merghadi, A.; Sahana, M.; Zhu, Z.; Chen, C.; Khosravi, K.; Yang, Y.; Pham, B. Assessment of advanced random forest and decision tree algorithms for modeling rainfall-induced landslide susceptibility in the Izu-Oshima Volcanic Island, Japan. *Sci. Total Environ.* **2019**, *662*, 332–346. [[CrossRef](#)] [[PubMed](#)]
8. Wu, X.; Shen, S.; Niu, R. Applying PSO-SVM model to predict landslide susceptibility under GIS support. *J. Wuhan Univ. (Inf. Sci. Ed.)* **2016**, *41*, 665–671.
9. Zhang, T.; Han, L.; Han, J.; Li, X.; Zhang, H.; Wang, H. Assessment of Landslide Susceptibility Using Integrated Ensemble Fractal Dimension with Kernel Logistic Regression Model. *Entropy* **2019**, *21*, 218. [[CrossRef](#)] [[PubMed](#)]
10. He, Y.; Zhao, Z.; Yang, W.; Yan, H.; Wang, W.; Sheng, Y.; Zhang, L.; Tao, L. A unified network of information considering superimposed landslide factors sequence and pixel spatial neighbourhood for landslide susceptibility mapping. *Int. J. Appl. Earth Obs. Geoinf.* **2021**, *104*, 102508. [[CrossRef](#)]
11. Ju, Y. Early Recognition of Loess Landslide Based on UAV Photogrammetry A Case Study of Heifangtai. Master's Thesis, Chengdu University of Technology, Chengdu, China, 2017.
12. Ghorbanzadeh, O.; Blaschke, T.; Gholamnia, K.; Meena, S.; Tiede, D.; Aryal, J. Evaluation of different machine learning methods and deep-learning convolutional neural networks for landslide detection. *Remote Sens.* **2019**, *11*, 196. [[CrossRef](#)]
13. Fang, R.; Liu, Y.; Huang, Z. Summary of regional landslide risk assessment methods based on machine learning. *Chin. J. Geol. Hazard Prev.* **2021**, *4*, 5–12.
14. Qiu, D. Study on Landslide Risk Assessment Based on Multi-Source Spatio-Temporal Data. Ph.D. Thesis, China University of Geosciences, Wuhan, China, 2017.
15. Zhao, C.; Qian, L. Comparative Study of Supervised and Unsupervised Classification in Remote Sensing Image. *J. Henan Univ. (Nat. Sci.)* **2004**, *34*, 90–93.
16. Zhou, P.; Cheng, J.; Yao, X.; Han, J. Machine Learning Paradigm in High Resolution remote Sensing Image interpretation. *J. Remote Sens.* **2021**, *25*, 182–197. [[CrossRef](#)]
17. Li, A.S.; Shi, W.X.; Zhang, Y.K. Genesis Analysis of the Landslide in Lanzhou and the Prevention and Control. *Subgrade Eng.* **2018**, *6*, 226–229.
18. Yan, Y.; Dong, X.; Li, Y. The comparative study of Remote Sensing Image Supervised classification methods based on ENVI. *Beijing Surv. Mapp.* **2011**, *3*, 14–16.
19. Wang, Y.; Wen, B. Study on geological hazard risk of landslides in Lanzhou. *Chin. Geol.* **2011**, *38*, 1593–1598.
20. Wu, W.; Feng, X.; Wang, Z.; Wang, W. Landslide and debris flow disaster and its prevention in Lanzhou. *J. Xi'an Inst. Geosci.* **1996**, *18*, 43–50.
21. Zhao, Z.; Wang, J.; Mao, X.; Ma, W.; Lu, W.; He, Y.; Gao, X. Landslide susceptibility assessment method coupled with multi-dimensional CNN. *J. Wuhan Univ. (Inf. Sci. Ed.)* **2023**.
22. He, Y.; Huang, Y.; Li, H.; Liu, Q.; Liu, G.; Zhou, Z.; Zhang, C. Random forest land cover classification based on Sentinel-2A image feature optimization. *Resour. Sci.* **2019**, *41*, 992–1001.
23. Revel, C.; Lonjou, V.; Marcq, S.; Desjardins, C.; Fougne, B.; Coppolani, C.; Guillemot, N.; Lacamp, A.; Lourme, E.; Miquel, C.; et al. Sentinel-2A and 2B absolute calibration monitoring. *Eur. J. Remote Sens.* **2019**, *52*, 122–137. [[CrossRef](#)]
24. Pham, B.T.; Tien Bui, D.; Pourghasemi, H.R.; Indra, P.; Dholakia, M. Landslide susceptibility assessment in the Uttarakhand area (India) using GIS: A comparison study of prediction capability of naive bayes, multilayer perceptron neural networks, and functional trees methods. *Theor. Appl. Climatol.* **2017**, *128*, 255–273. [[CrossRef](#)]
25. Luna-Alvarez, A.; Mujica-Vargas, D.; Matuz-Cruz, M.; Kinani, J.; Ramos-Díaz, E. *Self-Driving through a Time-Distributed Convolutional Recurrent Neural Network*; IEEE: Piscataway, NJ, USA, 2020.

26. Chauhan, S.; Sharma, M.; Arora, M.K.; Gupta, N.K. Landslide susceptibility zonation through ratings derived from artificial neural network. *Int. J. Appl. Earth Obs. Geoinf.* **2010**, *12*, 340–350. [[CrossRef](#)]
27. Guo, P.; Ai, Y.; Chen, C.; Li, W.; Wang, Q.; Pei, J. Effects of plant soil types on physicochemical properties and microbial activity of artificial soil on rock slope. *J. Soil Water Conserv.* **2012**, *26*, 6.
28. Cao, P. Study on Formation Mechanism and Stability of Baige High Landslide in Eastern Tibet. Master's Thesis, Kunming University of Science and Technology, Kunming, China, 2021.
29. Pu, H. InSAR Technology Based on Improved DBN Zhouqu County landslide Susceptibility Assessment. Master's Thesis, Lanzhou Jiaotong University, Lanzhou, China, 2022.
30. Sun, C.; Wu, Z.; Lv, Z.; Yao, N.; Wei, J. Quantifying different types of urban growth and the change dynamic in Guangzhou using multi-temporal remote sensing data. *Int. J. Appl. Earth Obs. Geoinf.* **2013**, *21*, 409–417. [[CrossRef](#)]
31. Li, A.; Hou, S.; Zhou, P. Study on rainfall-induced landslides in Yucheng District, Yaan City, Sichuan Province. *Chin. J. Geol. Hazards Prev.* **2007**, *18*, 15–17.
32. Zheng, Y.; Chen, J.; Wang, C.; Cheng, T. Application of certainty coefficient and stochastic forest model to the vulnerability assessment of landslides in Mangshi, Yunnan. *Geol. Sci. Technol. Bull.* **2020**, *39*, 131–144.
33. Tu, E.; Yang, J. An overview of semi-supervised learning theory and its research progress. *J. Shanghai Jiaotong Univ.* **2018**, *52*, 1280–1291.
34. Li, H.; Sun, Z.; Wu, Y.; Song, Y. Semi-supervised point cloud segmentation using self-training with label confidence prediction. *Neurocomputing* **2021**, *437*, 227–237. [[CrossRef](#)]
35. Zoph, B.; Ghiasi, G.; Lin, T.Y.; Yin, C.; Liu, H.; Cubuk, E.; Le, Q. Rethinking pre-training and self-training. *Adv. Neural Inf. Process. Syst.* **2020**, *33*, 3833–3845.
36. Ning, X.; Wang, X.; Xu, S.; Cai, W.; Zhang, L.; Yu, L.; Li, W. A review of research on co-training. *Concurr. Comput. Pract. Exp.* **2021**, *35*, e6276. [[CrossRef](#)]
37. Tran, H.Q.; Ha, C. Reducing the burden of data collection in a fingerprinting-based VLP system using a hybrid of improved co-training semi-supervised regression and adaptive boosting algorithms. *Opt. Commun.* **2021**, *488*, 126857. [[CrossRef](#)]
38. Wang, K.; Gou, C.; Duan, Y.; Lin, Y.; Zheng, X.; Wang, F. Research progress and prospect of generative countermeasure network GAN. *J. Autom.* **2017**, *43*, 321–332.
39. Lv, H.; Yu, L.; Zhou, X.; Deng, X. A review of semi-supervised deep learning image classification methods. *Comput. Sci. Explor.* **2021**, *15*, 1038–1048.
40. Goodfellow, I.; Pouget-Abadie, J.; Mirza, M.; Bing, X.; Warde-Farley, D.; Ozair, S.; Courville, A.; Bengio, Y. Generative adversarial networks. *Commun. ACM* **2020**, *11*, 139–144. [[CrossRef](#)]
41. Lin, Y.L.; Dai, X.Y.; Li, L.; Wang, X.; Wang, F. The New Frontier of AI Research: Generative Adversarial Networks. *Acta Autom. Sin.* **2018**, *44*, 775–792.
42. Liang, J.; Wei, J. Summary of generating countermeasure network GAN. *Comput. Sci. Explor.* **2020**, *14*, 1–17.
43. Zhou, T.; Liu, W.; Zhou, C.; Chen, L. *GAN-Based Semi-Supervised for Imbalanced Data Classification*; IEEE: Piscataway, NJ, USA, 2018.
44. Miao, X.; Wu, Y.; Wang, J.; Mao, Y.; Yin, X.; Jian, W. Generative Semi-Supervised Learning for Multivariate Time Series Imputation. Proceedings of the *AAAI Conf. Artif. Intell.* **2021**, *35*, 8983–8991. [[CrossRef](#)]
45. Ren, S.; He, K.; Girshick, R.; Sun, J. Faster R-CNN: Towards Real-Time Object Detection with Region Proposal Networks. *IEEE Trans. Pattern Anal. Mach. Intell.* **2017**, *39*, 1137–1149. [[CrossRef](#)] [[PubMed](#)]
46. Kyriou, A.; Nikolakopoulos, K. Landslide mapping using optical and radar data: A case study from Aminteo, Western Macedonia Greece. *Eur. J. Remote Sens.* **2020**, *53* (Suppl. 2), 17–27. [[CrossRef](#)]
47. Dille, A.; Kervyn, F.; Handwerker, A.L.; d'Oreye, N.; Derauw, D.; Mugaruka, B.; Samsonov, S.; Malet, J.; Kervyn, M.; Dewitte, O. When image correlation is needed; unravelling the complex dynamics of a slow-moving landslide in the tropics with dense radar and optical time series. *Remote Sens. Environ.* **2021**, *258*, 112402. [[CrossRef](#)]
48. Wang, Y.; Fang, Z.; Wang, M.; Peng, L.; Hong, H. Comparative study of landslide susceptibility mapping with different recurrent neural networks. *Comput. Geosci.* **2020**, *138*, 104445. [[CrossRef](#)]
49. Chen, W.; Peng, J.; Hong, H.; Shahabi, H.; Pradhan, B.; Liu, J.; Zhu, A.; Pei, X.; Duan, Z. Landslide susceptibility modelling using GIS—Based machine learning techniques for Chongren county, Jiangxi Province, China. *Sci. Total Environ.* **2018**, *626*, 1121–1135. [[CrossRef](#)] [[PubMed](#)]
50. He, Y.; Yao, S.; Yang, W.; Yan, H.; Zhang, L.; Wen, Z.; Zhang, Y.; Liu, T. An Extraction Method for Glacial Lakes Based on Landsat-8 Imagery Using an Improved U-Net Network. *IEEE J. Sel. Top. Appl. Earth Obs. Remote Sens.* **2021**, *14*, 6544–6558. [[CrossRef](#)]
51. Jiri, W.J.; Tian, H.; Han, J. Vulnerability evaluation of earthquake landslides based on different machine learning algorithms—taking Ludian earthquake as an example. *J. Kunming Univ. Sci. Technol. (Nat. Sci. Ed.)* **2022**, *47*, 47–56.

Disclaimer/Publisher's Note: The statements, opinions and data contained in all publications are solely those of the individual author(s) and contributor(s) and not of MDPI and/or the editor(s). MDPI and/or the editor(s) disclaim responsibility for any injury to people or property resulting from any ideas, methods, instructions or products referred to in the content.